

β -Skeleton Analysis of the Cosmic Web

Feng Fang¹, Jaime Forero-Romero², Graziano Rossi³, Xiao-Dong Li^{1,*}, Long-Long Feng¹

¹ School of Physics and Astronomy, Sun Yat-Sen University, Guangzhou 510297, P. R. China

² Departamento de Física, Universidad de los Andes, Cra. 1 No. 18A-10 Edificio Ip, CP 111711, Bogotá, Colombia

³ Department of Physics and Astronomy, Sejong University, Seoul, 143-747, Korea *corresponding author: lixiaod25@mail.sysu.edu.cn

7th September 2018

ABSTRACT

The β -skeleton is a mathematical method to construct graphs from a set of points that has been widely applied in the areas of image analysis, machine learning, visual perception, and pattern recognition. In this work, we apply the β -skeleton to study the cosmic web. We use this tool on observed and simulated data to identify the filamentary structures and characterize the statistical properties of the skeleton. In particular, we compare the β -skeletons built from SDSS-III galaxies to those obtained from MD-PATCHY mocks, and also to mocks directly built from the Big MultiDark N -body simulation. We find that the β -skeleton is able to reveal the underlying structures in observed and simulated samples without any parameter fine-tuning. A different degree of sparseness can be obtained by adjusting the value of β ; in addition, the statistical properties of the length and direction of the skeleton connections show a clear dependence on redshift space distortions (RSDs) and galaxy bias. We also find that the N -body simulation accurately reproduces the RSD effect in the data, while the MD-PATCHY mocks appear to underestimate its magnitude. Our proof-of-concept study shows that the statistical properties of the β -skeleton can be used to probe cosmological parameters and galaxy evolution.

Key words: Cosmology: cosmological parameters – observations – large-scale structure of universe; Methods: statistical

1 INTRODUCTION

The spatial distribution of the nearest galaxies on scales of a few hundred Megaparsecs follows a distinct filamentary motif. This pattern is known as ‘cosmic web’ (Bardeen et al. 1986), and it has been observed at different cosmic epochs (de Lapparent et al. 1986; Huchra et al. 2012; Tegmark et al. 2004; Guzzo et al. 2014). The search of consistent and stable methods to define this web-like structure has been the subject of continuous research for the last ~ 40 years, since its existence was confirmed in early cosmic maps from galaxy redshift surveys. The cosmic web has also been detected in the dark matter description provided by cosmological simulations – see Libeskind et al. (2018) for a recent review.

The cosmic web is usually classified into four different components: halos, sheets, filaments, and voids. Many algorithms are focused in finding the two most prominent web features present in redshift galaxy surveys: voids and filaments. Voids are regions with sizes in the range of 20 – 50 Mpc, practically devoid of galaxies – see van de Weygaert (2016) for a recent review of void finding algorithms. Filaments appear to be the main bridges connecting high-density

regions. On the largest scales, the filament length can be on the order of 10 – 100 Mpc.

The emergence of the cosmic web can be understood as the interplay of two conditions. First, the initial Gaussian random density field; second, its evolution under gravity. In fact, the initial anisotropies in the density field are amplified by gravity to finally become filaments and voids. The structure of the cosmic web is thus expected to encode information about the underlying cosmological model: namely, type of initial fluctuations, proportions of different kinds of matter, the expansion history of the Universe, and the rules of gravity. Voids, for instance, can be used as cosmological probes, as their structure is strongly influenced by dark energy (Lee & Park 2009; Bos et al. 2012); and the statistical isotropy of filaments can be used to perform the Alcock-Paczynski (AP) test (Li et al. 2014a).

In this paper, we introduce the β -skeleton as an algorithm to characterize the cosmic web. The β -skeleton concept stems from the fields of computational geometry and geometric graph theory and has been widely applied in the areas of image analysis, machine learning, visual perception, and pattern recognition (Edelsbrunner et al. 1983; Amenta et al. 1998; Zhang & King 2002). In the context of

arXiv:1809.00438v2 [astro-ph.CO] 6 Sep 2018

web finders, the β -skeleton belongs to a class of algorithms that, starting from a set of 3D spatial points, builds a graph describing the degree of connectedness. In this aspect, it is similar to the minimum spanning tree (MST) algorithm (Barrow et al. 1985), with the main difference that the resulting graph depends on the continuous β parameter; it is also related to web finders that are designed on the basis of topological persistence, such as DisPerSE (Sousbie 2011).

This paper is organized as follows. In Section 2, we briefly introduce the definition and the basic properties of the β -skeleton. In Section 3, we describe the Big MultiDark Planck (BigMDPL) simulation and the SDSS-III BOSS Data Release 12 (DR12) galaxy sample, which are used later on in the analysis. The application of the β -skeleton statistics is presented in Section 4, where we discuss the dependence of the skeleton on the values of β , on the redshift of the various samples, on the redshift-space distortions (RSDs), and on the cosmological volume and AP effects; we also graphically illustrate the β -skeleton constructed from SDSS-III BOSS DR12 galaxies, and eventually compare the skeletons obtained from observational data and simulated catalogs. Finally, we summarize our findings and conclude in Section 5.

2 β -SKELETON: THEORY

In what follows, we define the β -skeleton and briefly explain how it is used to study the statistical properties of the large-scale structure (LSS) of the universe; for more details about the β -skeleton in topology and in geometric graph theory, please refer to Kirkpatrick & Radke (1985); Correa & Lindstrom (2012).

For a point set S in a n -dimensional Euclidean space, the β -skeleton defines an *edge set* so that for any two points p and q in S , those points are considered to be connected if there is not a third point r in the various *empty regions* shown in Figure 1 with dotted lines. Specifically:

- For $0 < \beta < 1$, the *empty region* is the intersection of all the spheres with diameter d_{pq}/β , having p and q on their boundary.
- For $\beta = 1$, the *empty region* is the sphere with diameter d_{pq} .
- For $\beta \geq 1$, the *empty region* is defined in two different ways: namely, the *Circle-based* definition and the *Lune-based* definition (see again Figure 1 for details). In this paper, we adopt the latter one, according to which the *empty region* R_{pq} is the intersections of two spheres with diameter βd_{pq} and centered at $p + \beta(q-p)/2$ and $q + \beta(p-q)/2$, respectively.

The β -skeleton defined above has several interesting mathematical properties. As β varies continuously from 0 to ∞ , the constructed graphs change from a complete graph to an empty graph. The special case of $\beta = 1$ leads to the so called "Gabriel graph", which is known to contain the Euclidean minimum spanning tree.¹ The β -skeleton has several important applications in computational science and graphical theory. For example, in image analysis, it was used to

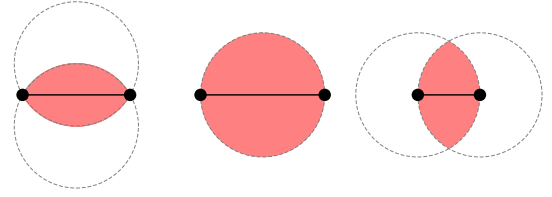


Figure 1. Empty region of the β -skeleton under the Lune-based definition. Left: $\beta < 1$, Middle: $\beta = 1$, Right: $\beta > 1$

reconstruct the shape of a two-dimensional object given a set of sample points on the boundary of the object: this is because the $\beta = 1.7$ *Circle-based* graphs have been proven to correctly reconstruct the entire boundary of any smooth surface, without generating any edges that do not belong to the boundary – as long as the samples are sufficiently dense with respect to the local curvature of the surface.² The β -skeleton has also been applied in machine learning systems, in order to solve geometric classification problems (Zhang & King 2002; Toussaint 2005). In wireless ad hoc networks, for controlling the communication complexity, the β -skeleton was used as a mechanism to choose a subset of the pairs of wireless stations that can communicate with each other (Bhardwaj et al. 2005). In visual perception and pattern recognition, it was used to find families of proximity graphs (Ersoy et al. 2011). For more details about the application of the β -skeleton, see e.g. Bose et al. (2002); Wang (2008); Lafarge & Alliez (2013).

3 OBSERVED AND SIMULATED DATASETS

First, we test our method using the BigMDPL simulation. The BigMDPL belongs to the series of MultiDark N -body simulations with Planck 2015 cosmology, thoroughly described in Klypin et al. (2016). It is characterized by a box with $2.5h^{-1}\text{Gpc}$ on a side, with 3840^3 dark matter particles, providing a mass resolution of $2.4 \times 10^{10} h^{-1} M_{\odot}$. The initial conditions, based on primordial Gaussian fluctuations, are generated via the Zel'dovich approximation at $z_{\text{init}} = 100$. The cosmology assumed is a flat ΛCDM model with $\Omega_m = 0.307115$, $\Omega_b = 0.048206$, $\sigma_8 = 0.8288$, $n_s = 0.9611$, and $H_0 = 67.77 \text{ km s}^{-1} \text{Mpc}^{-1}$.

We then apply the β -skeleton statistics to the Baryon Oscillation Spectroscopic Survey (BOSS) DR12 CMASS galaxy sample. BOSS (Dawson et al. 2012; Smee et al. 2013), is the cosmological counterpart of the Sloan Digital Sky Survey III (SDSS-III; Eisenstein et al. 2011), and it is still one of the largest spectroscopic galaxy surveys to date. It has obtained spectra and redshifts of about 1.37 million galaxies selected from the SDSS imaging up to $z = 0.7$. The Northern and Southern Sky footprints cover an area of $\sim 10,000$ square degrees, and the galaxy samples are conventionally split into the LOWZ catalog at $z < 0.43$ and the CMASS catalog covering the redshift interval $0.43 \leq z \leq 0.7$ (Reid

¹ minimum spanning tree of a set of n points in the plane where the weight of the edge between each pair of points is the Euclidean distance between those two points.

² In experimental testing, $\beta = 1.2$ was more effective in reconstructing street maps from a set of points, marking the center lines of the streets in a geographic information system.

et al. 2015). In this work, we only use the CMASS sample at $0.43 \leq z \leq 0.7$, which contains ~ 0.77 million galaxies.

In order to compare observational data with N -body simulation predictions, we use the MD-PATCHY mocks available for the BOSS survey. The MD-PATCHY mocks (Kitaura et al. 2016; Rodríguez-Torres et al. 2016) adopt an halo abundance matching technique to reproduce the two- and three-point clustering measurements of BOSS. The redshift evolution of the biased tracers is matched to the corresponding observations by applying the aforementioned technique in a number of redshift bins, with the resulting mock catalogs being combined together to form a contiguous lightcone. The MD-PATCHY mocks are constructed to reproduce the number density, selection function, and survey geometry of the BOSS DR12 catalog; moreover, the two-point correlation function (2PCF) of the observational data is correctly recovered down to a few Mpc scales, in general within 1σ error (Kitaura et al. 2016). The MD-PATCHY mocks have been carefully tested and subsequently adopted for the statistical analysis of BOSS data in a series of works – see for example Alam et al. (2017), and references therein.

4 MAIN RESULTS

4.1 An Illustrative Application

As an illustrative example, we first apply the β -skeleton statistics to a set of LSS mock samples using $\beta = 1, 3, 10$, respectively. We do this as follows: essentially, we simply take the $z = 0$ halo catalog of the BigMDPL simulation and apply a mass cut $M > 1 \times 10^{13} M_\odot$ and a radial cut $r_{cut} < 500 h^{-1} \text{Mpc}$. This procedure allows us to create a shell-shaped sample containing 30,000 dark matter halos. In order to make comparisons with an unclustered distribution, we also built a random sample with the same size, shape, and number of points as the previous mock realizations.

Results of this test are displayed in Figures 2 and 3, where we show the skeletons of the mock samples using $\beta = 1, 3, 10$, respectively (from top to bottom) – as well as the skeleton of the random sample when $\beta = 3$. In all cases, the left panels display a $200 \times 200 \times 30 h^{-1} \text{Mpc}$ slice of the samples with connections (red lines), while the right panels show histograms of the length of the connections L (upper part) and the cosine of the angle between the line-of-sight (LOS) and the connection line, $\mu \equiv |\cos\theta|$ (lower part).

Clearly, the amount of connections is smaller when β is larger. This is evident from the definition for the β -skeleton presented in Figure 1, which shows an increment of the empty region with β ; namely, the threshold for having two particles connected becomes more strict. In particular, when $\beta = 1$ we find $\sim 80,000$ connections, far more than the number of points of the sample, while we detect only 15,000 connections when $\beta = 10$.

The β -skeleton automatically generates filament-like structures from the point sample; this is most clearly detected when $\beta = 3$, as can be seen in Figure 2. For example, in the upper-left panel one can notice that ~ 20 galaxies naturally arise from a long straight filament-shape structure: this structure is then identified, and those galaxies are linked together. The straight line ends at $(x, y) \approx (25, 140) h^{-1} \text{Mpc}$,

while the structure continues and extends up to $y = 60 h^{-1} \text{Mpc}$. It then bifurcates at $y \approx 110 h^{-1} \text{Mpc}$, and further extends to the left, lower-left, and right side of the graph, forming a larger connected structure which captures $\approx 70\%$ of the galaxies shown in the panel. Also, some of those galaxies act as “knots” of the structure (i.e., three or more galaxies are connected). For example, the “knots” galaxy at $(x, y) \approx (25, 140) h^{-1} \text{Mpc}$ links together the up-down filament at its left to the galaxies at the right. Moreover, there are also isolated structures having a relatively small number of group members – see for instance ~ 25 galaxies distributed around $(x, y) \approx (100, 150) h^{-1} \text{Mpc}$ that form an “A”-shaped structure.

Altering the values of β has a strong influence on the overall shape of the skeleton graphs. For example, the case of $\beta = 1$ roughly corresponds to computing the 2PCF, in the sense that many connections are generated, regardless of whether or not those connections lie within a filament. When $\beta = 3$, the set of structures generated is much closer to the observed cosmic web, meaning that the number of connections is comparable to the number of actual galaxies. For $\beta = 10$, one gets a very sparse graph as expected, since only the small and relatively isolated compact groups of galaxies are identified and connected.

The statistical properties of the connection length L also vary with β . For larger values of β , L gets smaller and appears to be more concentrated – this is because, due to a tight threshold, it is difficult to connect two points separated by a large distance. From the figure, we infer that the mean length is $\bar{L} = 6.14, 3.17, 1.97 h^{-1} \text{Mpc}$ when $\beta = 1, 3, 10$, respectively.

For $\beta = 3$, we then compare the results obtained from the mock samples with those derived from the unclustered (random) distribution. As expected, we find that the random sample exhibits “structures” chaotic in shape; moreover, due to a lack of compact structures, the distribution of L inferred from the random sample has a mean $\bar{L} = 4.55$, a value much larger than those obtained from the mock samples.

Finally, as shown in all the bottom right panels of Figures 2 and 3, we find that $\mu \sim 0.5$ within the corresponding errorbars, implying that the directions of the connections are always randomly distributed, with no preferred orientation.

4.2 Redshift Evolution

Next, we study in detail the statistical properties of the β -skeletons constructed from N -body simulations. We analyze 4 BigMDPL snapshots at redshifts 0, 0.3, 0.6, and 0.9, respectively, and consider both cases with and without RSD effects. Moreover, we impose a mass cut $M < 1 \times 10^{13} M_\odot$ and a radial cut $r < 2500 h^{-1} \text{Mpc}$, yielding a number of galaxies $N_{gal} = 3.85, 3.37, 2.71, 2.07$ (in units of millions) at those 4 redshifts, respectively.

Results are displayed in Figure 4. Specifically, the upper-right panel shows the histogram of the connecting length L , assuming that the *real space positions* of galaxies are used to construct the skeleton (i.e., no RSD involved). With this assumption, our main findings are summarized as follows:

- The distribution of the connecting length peaks at $1.5 - 1.8 h^{-1} \text{Mpc}$. This represents the typical separation

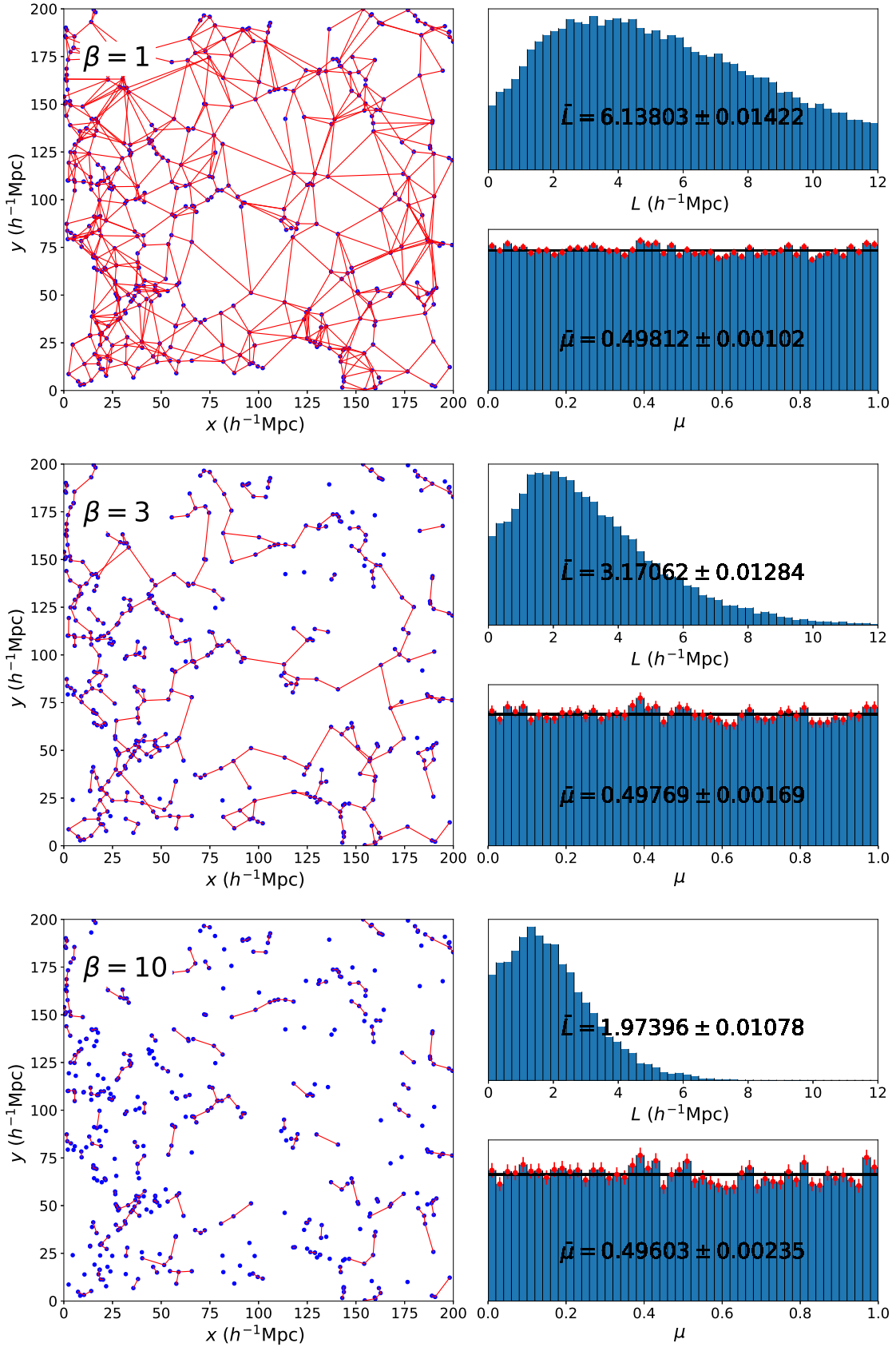


Figure 2. An illustrative example. Application of the β -skeleton statistics to a set of LSS mock samples when $\beta = 1, 3, 10$, respectively. In the figure, the left panels show the skeletons of the mock samples for different values of β , while the right panels present the statistics of the length of the connections (upper parts) and the orientations of those connections (lower parts). See the main text for more details.

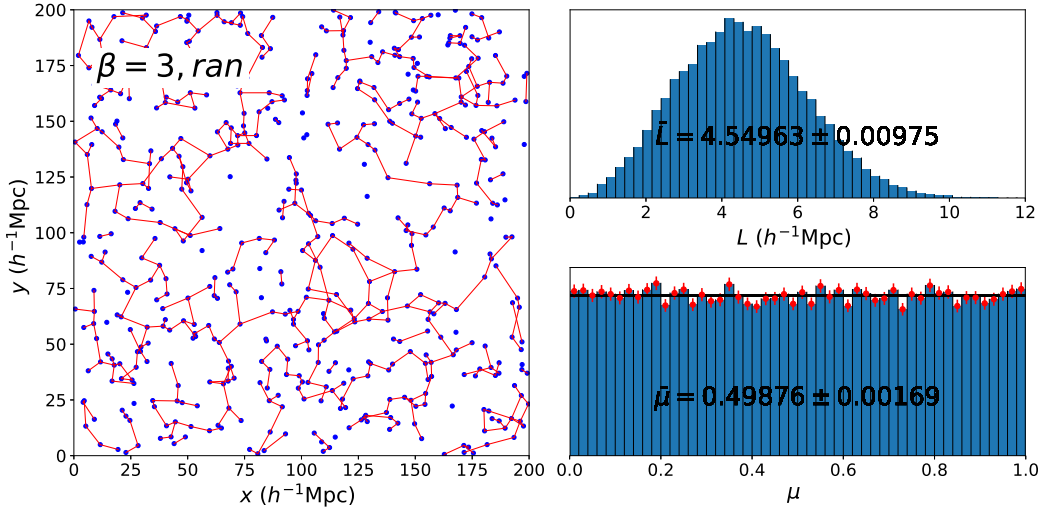


Figure 3. Same as the previous figure when $\beta = 3$, but for an unclustered (random) distribution.

length between galaxies in the skeleton. Above (below) the peak scale, N decreases with increasing (decreasing) L ; a secondary peak appears at $0.1 - 0.2 h^{-1}\text{Mpc}$, due to the fact that there is a large number of compact clusters at this scale.

- As the redshift increases, the number of connections decreases with decreasing N_{gal} . Again, the total number of connections, which is found to be 3.74, 3.27, 2.62, 2.00 at $z = 0.9, 0.6, 0.3, 0.0$, respectively, scales with N_{gal} .

- The 4 distributions (indicated in the panel with different colors) merge at $L \approx 8 h^{-1}\text{Mpc}$. Above this scale, the $z = 0.9$ sample shows the largest number of connections (even if the corresponding N_{gal} is significantly smaller compared to the other three samples), which is a clear signal that the constructed structures in this sparse sample have larger sizes – namely, at lower redshifts, objects become more compact and the distribution shifts to smaller L as structures grow.

The upper-left panel in Figure 4 displays the L -distribution, but now using the *redshift space positions* of the same galaxies considered before. In this case, the peculiar velocity of galaxies perturbs their observed redshifts via

$$\Delta z = (1+z) \frac{v_{\text{LOS}}}{c}, \quad (1)$$

where v_{LOS} is the line-of-sight (LOS) component of the velocity. The distortion of z leads to a corresponding distortion in the inferred galaxy distances, known as the RSD effect. At small scales ($\lesssim 5 h^{-1}\text{Mpc}$), this leads to the finger of god (FOG) feature (Jackson 1972) (i.e., a stretch of structures along the LOS) due to chaotic small-scale motions of galaxies in the non-linear regime. At large scales ($\gtrsim 40 h^{-1}\text{Mpc}$), the RSD effect is known as the ‘Kaiser effect’ (Kaiser 1987) (i.e., a compression of structures along the LOS), due to the coherent motions of galaxies driven by gravity.

Considering the previously reported measurements of L , we can infer that the skeletons constructed from the BigM-DPL simulation are mainly affected by the small-scale FOG effect. As a consequence, the number of short connections

characterized by $L \lesssim 1 h^{-1}\text{Mpc}$ is heavily suppressed, because of the stretch of distances among galaxies due to the FOG feature. Also, the secondary peak – found in the case where no RSD are considered – now disappears. The distribution still peaks around $1.5 h^{-1}\text{Mpc}$, but the height is $\sim 20\%$ higher than the one found in the no RSD case; this is because there is an extra contribution from the ‘spikes’ created by the FOG effect.

Finally, the lower panel in Figure 4 shows the histogram of μ at those four different redshifts previously specified, when RSD effects are present. As expected, we find a non-flat distribution due to anisotropies induced by RSDs; the FOG leads to a sharp increment of N at $\mu \rightarrow 1$, and the effect is stronger at lower redshifts.

4.3 Cosmological Effects

We then consider the effect of cosmological parameters on the β -skeleton statistics. To this end, suppose we are probing both the shape and volume of a celestial object by measuring its redshift span Δz and angular size $\Delta\theta$. We can compute its LOS dimensions in the radial (Δr_{\parallel}) and transverse (Δr_{\perp}) directions using the relations:

$$\Delta r_{\parallel} = \frac{c}{H(z)} \Delta z, \quad \Delta r_{\perp} = (1+z) D_A(z) \Delta\theta, \quad (2)$$

where H is the Hubble parameter and D_A is the angular diameter distance. For a flat ΛCDM model with constant dark energy equation of state (DE EoS) parameter w , H and D_A are simply expressed by:

$$H(z) = H_0 \sqrt{\Omega_m a^{-3} + (1 - \Omega_m)(1+z)^{3(1+w)}},$$

$$D_A(z) = \frac{1}{1+z} r(z) = \frac{1}{1+z} \int_0^z \frac{dz'}{H(z')}, \quad (3)$$

with H_0 the present value of the Hubble constant, and $r(z)$ the comoving distance.

If an incorrect set of cosmological parameters is chosen in the conversion defined by Equations (2) and (3), then the inferred Δr_{\parallel} and Δr_{\perp} would be both incorrect, resulting in a distorted shape (this is known as the ‘AP effect’) and in a

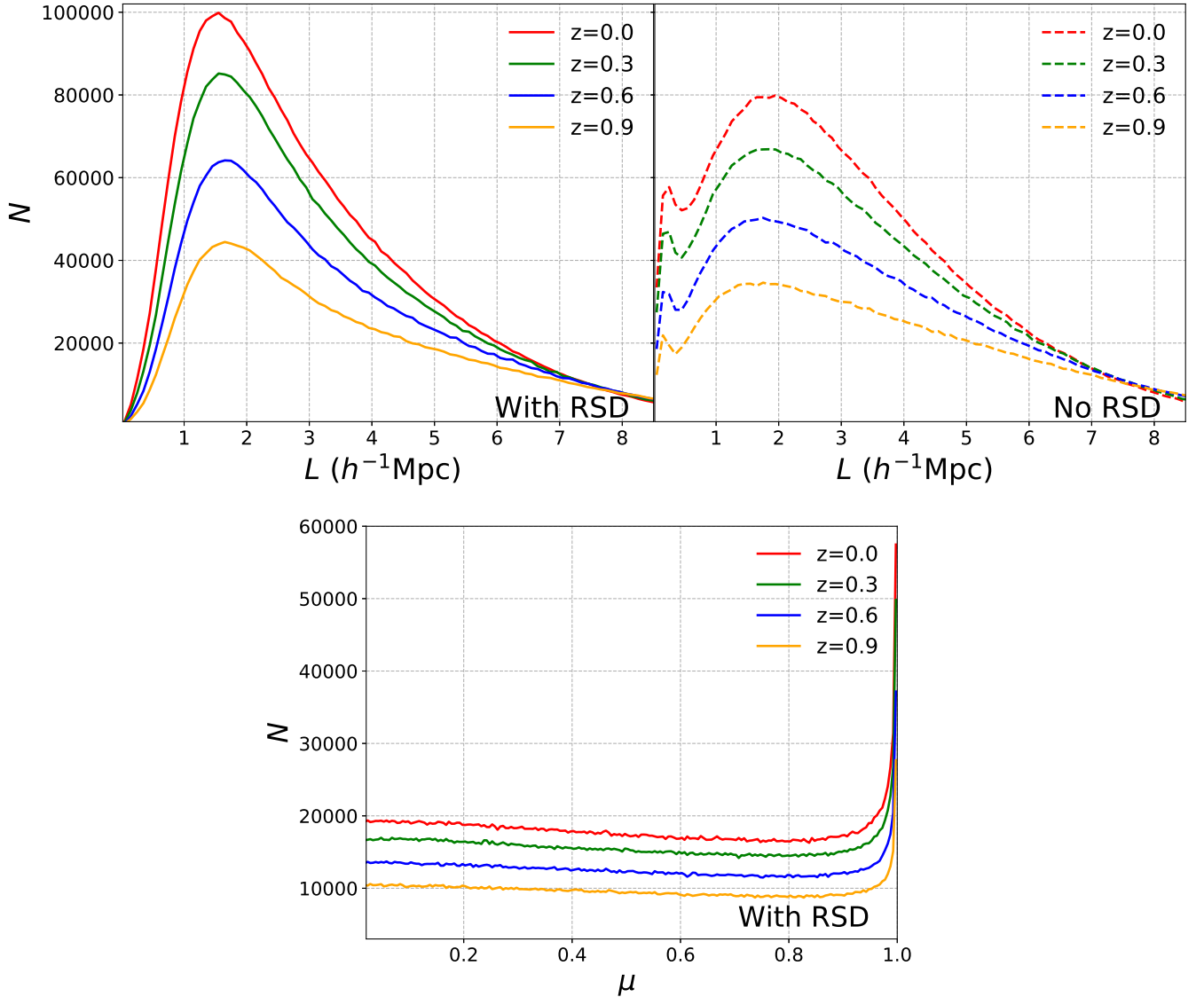


Figure 4. Histograms of the connecting lengths L with (top-left panel) and without (top-right panel) RSD effects. Those lengths are used to construct the corresponding skeleton structures, as explained in the main text. The lower panel shows the histogram of the directions of the connections μ at 4 different redshifts – as indicated in the plot with different colors – when RSD effects are included.

wrongly estimated volume (this is termed as ‘volume effect’) of the cosmological object. We can describe the magnitude of this combined effect via the relations:

$$\frac{[\Delta r_{\parallel}/\Delta r_{\perp}]_{\text{wrong}}}{[\Delta r_{\parallel}/\Delta r_{\perp}]_{\text{true}}} = \frac{[D_A(z)H(z)]_{\text{true}}}{[D_A(z)H(z)]_{\text{wrong}}}, \quad (4)$$

$$\frac{[\Delta r_{\parallel}(\Delta r_{\perp})^2]_{\text{wrong}}}{[\Delta r_{\parallel}(\Delta r_{\perp})^2]_{\text{true}}} = \frac{\text{Vol}_{\text{wrong}}}{\text{Vol}_{\text{true}}} = \frac{[D_A(z)^2/H(z)]_{\text{wrong}}}{[D_A(z)^2/H(z)]_{\text{true}}}, \quad (5)$$

where ‘true’ and ‘wrong’ denote the values of those measured quantities in the actual (‘true’) cosmology and in the incorrectly assumed cosmology, respectively. From the AP and the volume effects, we can therefore constrain the two quantities $D_A(z)H(z)$ and $D_A(z)^2/H(z)$. Clearly, these two effects will impact the statistical properties of the β -skeleton, which is sensitive to both the number density and the anisotropy of the cosmological sample in question.

In order to quantify the sensitivity of the AP and volume effects on the β -skeleton, we next apply the β -skeleton statistics to the $z = 0.6$ snapshot of the BigMDPL sample – but considering *different cosmologies*. Namely, we adopt five cosmological models characterized by $\Omega_m = 0.307115$ with $w = -1.0, -1.5, -0.5$, and $\Omega_m = 0.2, 0.4$ with $w = -1.0$, and infer the actual positions of the galaxy sample using those five cosmologies in turn. For all those cases, we then analyze the statistical properties of the connection length L and of the cosine of the orientation angle μ .

Our main results are shown in Figures 5 and 6. Specifically, Figure 5 displays the histograms of L : the left panel presents the statistical distribution in redshift space (with RSDs), while the right panel shows the analogous distribution but in real space (no RSDs). Also in these cases, we find similar properties as those highlighted in Figure 4 (e.g.,

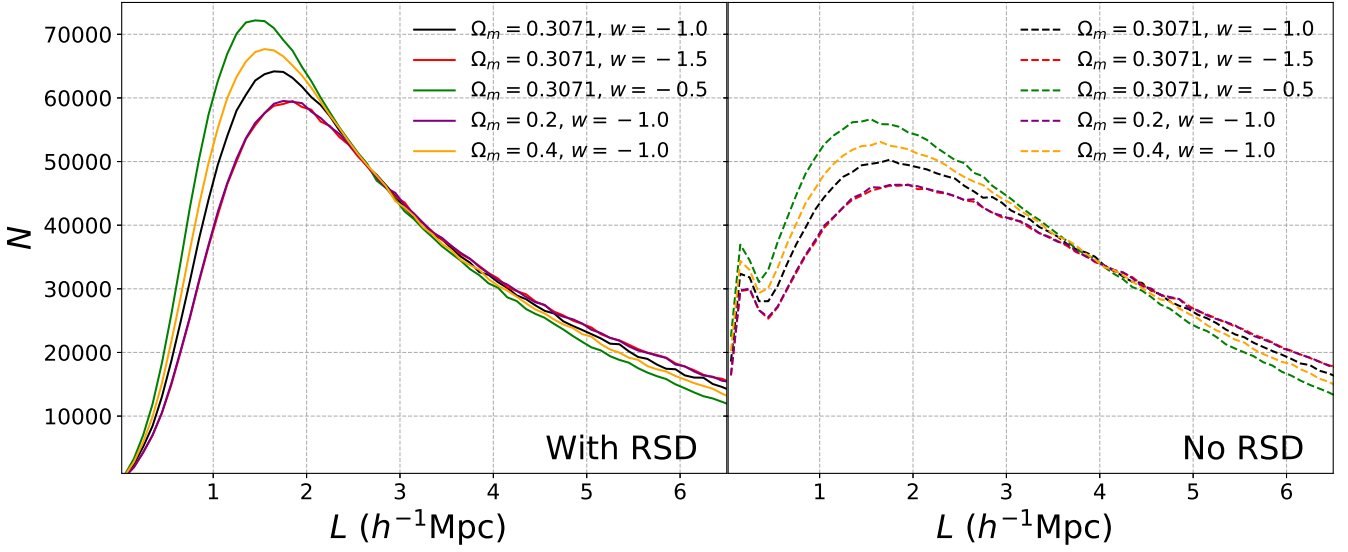


Figure 5. Sensitivity of the AP and volume effects on the β -skeleton: connecting length. Distribution of L in different cosmological models defined by Ω_m and w , as indicated in the various panels. The β -skeleton statistics is applied to the BigMDPL simulation snapshot at $z = 0.6$, when RSDs are considered (redshift space – left panel) or excluded (real space – right panel). Cosmological effects due to simultaneous variations in Ω_m and w are clearly detected.

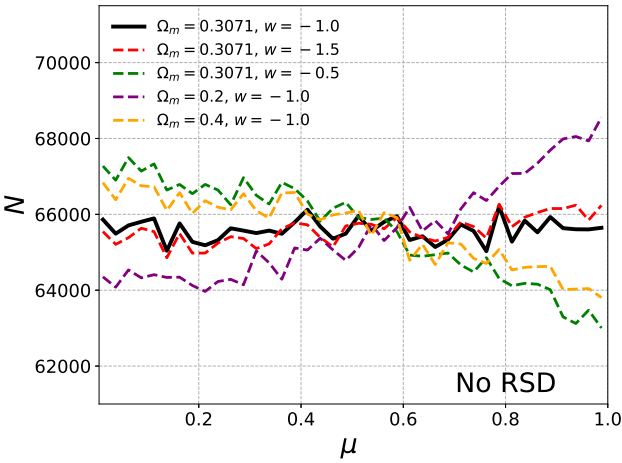


Figure 6. Sensitivity of the AP and volume effects on the β -skeleton: connecting direction. Distribution of μ in different cosmological models as in the right panel of the previous figure (no RSD effects), but now for the connecting direction. See the main text for more details.

two peaks when RSDs are not present, and one peak at $1.5 h^{-1}\text{Mpc}$ if RSDs are added).

Moreover, cosmological effects of varying Ω_m and w are clearly detected: the two cosmologies with $w = -1.5$ or $\Omega_m = 0.2$ are characterized by a faster expansion rate of the Universe compared to the ‘true’ cosmology. On the one hand, the comoving volume is overestimated – resulting in a distribution of L shifted to larger length; on the other hand, the overall LSS is stretched along the LOS because of the AP effect. Hence, the distribution of μ is enhanced (suppressed) in the region where $\mu > 0.5$ ($\mu < 0.5$), as evident

from Figure 6 – which shows only the case when RSDs are not included.³

In the other two considered cosmologies, the effect is the opposite: a shrinking of the volume size shifts L to smaller scales, and the compression of structures along the LOS tilts the distribution of μ , as expected.

4.4 Different Mass-Cut Effects

In the previous analysis we imposed a fixed mass-cut to all the BigMDPL snapshots considered, namely $M > 1 \times 10^{13} M_\odot$. We now explore the effect of a different mass-cut on the β -skeleton statistics. To this end, Figure 7 shows results of varying the mass cut (indicated with different color lines) at $z = 0$, when RSDs are also accounted for. In particular, we highlight the following findings:

- When selecting galaxies in the mass intervals $[4 \times 10^{12} - 6 \times 10^{12}] M_\odot$, $[6 \times 10^{12} - 8 \times 10^{12}] M_\odot$, $[2 \times 10^{13} - 5 \times 10^{13}] M_\odot$, and $[5 \times 10^{13} - 1 \times 10^{14}] M_\odot$, we obtain $N_{\text{gal}} = [6101837, 3142136, 2318205, 706430]$ and $L = [3.96, 5.12, 5.29, 8.23]$ – respectively. The relation $\bar{L} \propto N_{\text{gal}}^{-1/3}$ holds well.
- Samples characterized by a relatively smaller galaxy mass are dominated by satellite galaxies, and therefore they are more affected by the small-scale FOG effect – resulting in a significant peak around $\mu \simeq 1$.
- On the contrary, samples with relatively larger galaxy mass are more dominated by central galaxies. Hence, they are more affected by the Kaiser effect, and thus present a more significant tilt when $\mu < 0.8$. The peak near $\mu \sim 1$ is less significant, due to a much weaker FOG effect.

³ See Figure 1 of Li et al. (2014b, 2015) for a clearer explanations on the volume and AP effects in cosmologies with incorrect Ω_m or w values.

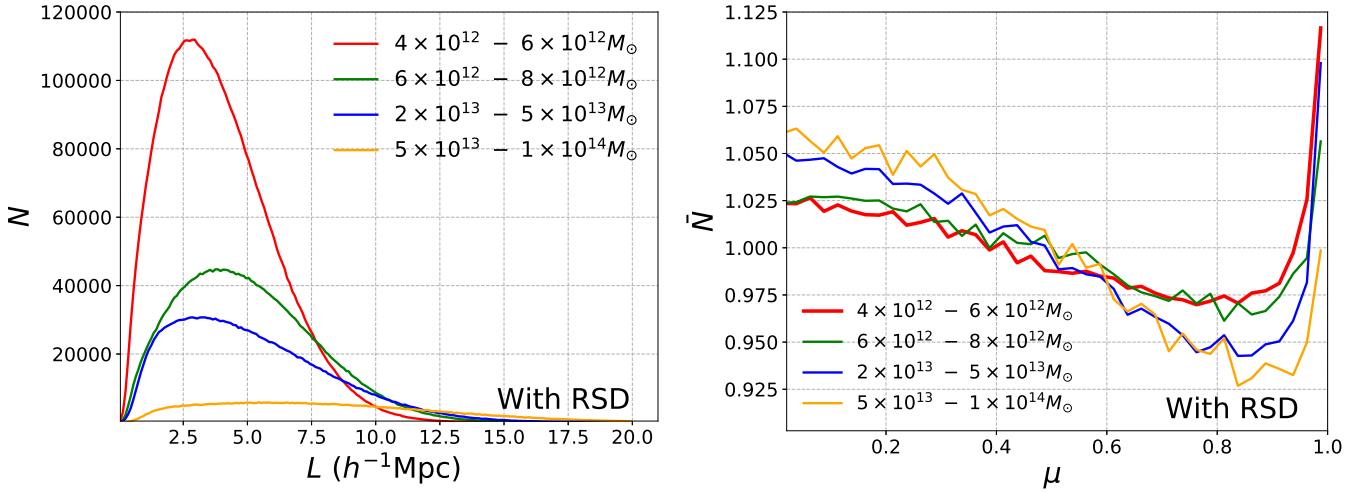


Figure 7. Mass-cut effects on the β -skeleton statistics. [Left] Distribution of the connecting length L as a function of different mass cuts, as indicated in the panel with different line-colors, when RSDs are included and $z = 0$. [Right] Same as in the left panel, but now for the connecting direction μ .

4.5 Observational Data: Comparisons

Finally, we apply the β -skeleton statistics to observational galaxy data, obtained from the SDSS-III BOSS Data Release 12 (DR12); in particular, we consider only the CMASS galaxy sample within $0.43 \leq z \leq 0.7$, which contains ~ 0.77 million galaxies. Results are shown in Figure 8. Specifically, the left panel shows all the Northern sky galaxies in the redshift shell $0.44 < z < 0.48$ – the specific redshift range has been chosen just for visualization purposes, and in the plot different colors indicate galaxies with different angular directions and distances. The right panel is a sub-patch enlargement of the left panel, where the coordinate cut is defined by $170 < \text{RA} < 210$ and $30 < \text{DEC} < 50$.

In addition, Figure 9 presents a comparison between the statistical properties of the β -skeleton as inferred from the SDSS-III BOSS CMASS galaxy sample, and of 4 mock MD-PATCHY realizations that are constructed to mimic the BOSS CMASS sample, plus a BigMDPL snapshot at $z = 0.6$. The main findings are as follows:

- The observed and simulated distributions of the connection lengths L are in good agreement. They both peak at $L \sim 1.5 h^{-1}$ Mpc, and decrease outside of this interval.
- The MD-PATCHY mocks generally underestimate the FOG effect, a fact evident if one looks towards the $\mu \rightarrow 1$ side of the lower panel in Figure 9.
- The μ distribution of BOSS galaxies is much closer to the one derived from the BigMDPL mock at $z = 0.6$, indicating that N -body simulations are capable of well-reproducing the RSD effect present in the data.

5 CONCLUDING REMARKS

5.1 Brief Summary

In this work, we performed a first investigation of the application of β -skeleton statistics to cosmic web data. We use the BigMDPL simulation as a testing sample, and study how the

constructed skeleton depends on the values of β , redshifts, RSD, AP and volume effects, and different and mass cuts. We find a significant variation of the length and direction of the cosmic web connections under different parameters and assumptions.

We then apply the β -skeleton method to SDSS-III BOSS DR12 CMASS galaxies, and compare our measurements with MD-PATCHY mocks. We find that the N -body sample provides a rather similar μ -distribution to the one of the data, implying that RSD effects of the sample are accurately reconstructed. On the contrary, the MD-PATCHY mocks appear to underestimate the magnitude of the FOG effect, although they are designed to correctly reproduce the 2- and 3-point correlation functions of the data.

The β -skeleton clearly reveals the underlying structures encoded in the sample of points. From its definition, we see that it does not require us to pre-select a specific scale (such as the linking length in the FoF algorithm). One can in fact adjust the value of β , and obtain a skeleton-like structure with different magnitudes of sparseness. Furthermore, the statistical properties of the β -skeleton depend on the RSD effect, on the AP and volume effects, and on galaxy bias. Hence, in turn they could be used as a statistical tool to characterize the magnitude of these effects.

5.2 Comparison with 2-Point Statistics

A standard cosmological analysis generally involves the computation of the 2PCF, and of 2-point-related statistics. In computing the 2PCF, one considers all the possible pairs of galaxies (restricted to some specific scale), and study their main clustering properties. Instead, the β -skeleton statistics focuses only on the small fraction of pairs which traces the structure; hence, the physical information is actually concentrated on a subset of galaxies. Also, the computation of the β -skeleton is much faster than the 2PCF, so it can be used as a complementary fast statistical tool to study the basic properties of a given sample.

Although the pairs that define the β -skeleton constitute

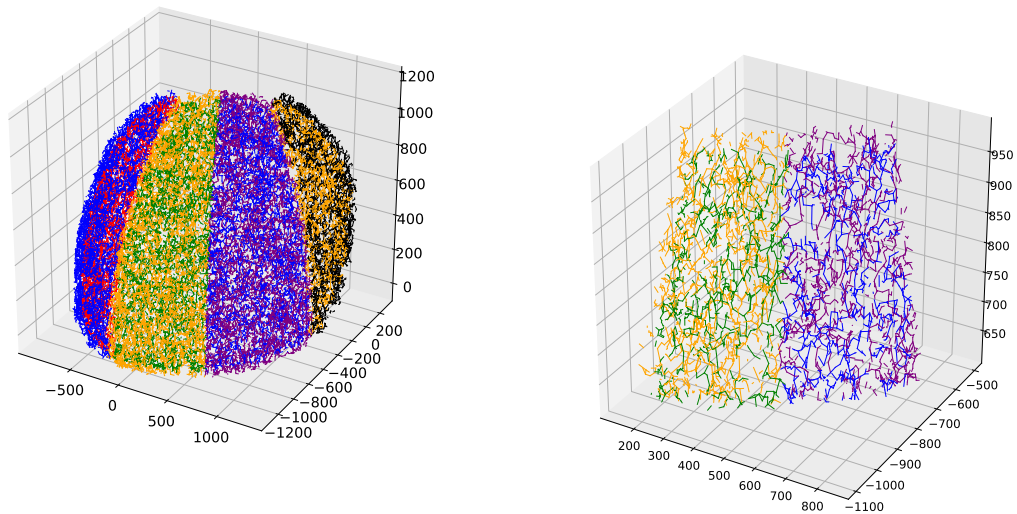


Figure 8. *Application of the β -skeleton to observational data.* [Left] Visualization of the skeleton mapped by SDSS-III CMASS BOSS galaxies within the redshift range $0.44 < z < 0.48$ in the Northern sky (in units of h^{-1} Mpc). Different colors indicate galaxies with different angular directions and distances. [Right]. Zoom into a sub-patch of the left panel, which clearly shows the structure of the observed β -skeleton. See the main text for more details.

a subset of those involved in the 2PCF calculations, one cannot conclude that the information derived from the β -skeleton analysis is just a subset of the one inferred from 2PCF measurements. For example, Figure 9 already reveals that the MD-PATCHY mocks, constructed to reproduce the 2PCF of the data, have instead a rather different β -skeleton statistics from the actual data.⁴

This is also one main reason to pursue a β -skeleton analysis: the 2-point statistics, although powerful, essentially compresses all the LSS information into histograms, while the cosmic web presents a much richer and complex structure that can only be revealed with higher-order, more detailed analysis.

5.3 Future Investigations

This work is a first attempt to apply the β -skeleton statistics to describe the cosmic web. Of course, our study can be further expanded in several directions. For instance, in this paper we only focused on the distribution of L and μ , in order to characterize the size and anisotropy of the LSS, but additional quantities can be used in future investigations. An example is represented by the number of connections linked at every galaxy, which allows us to study and weight the ‘knots’ (which connect together different filaments). Another possibility is to study how the connection lengths of galaxies differ depending on their environment. Namely, if

they are within a homogeneous structure such as cluster, their connection length values should be statistically close to unity, while for galaxies lying at the boundary of clusters and filaments we expect those values to deviate from unity; the magnitude of the deviation describes how sharp the LSS are transformed from cluster-like to filament-like structures.

Another possibility is to compare the β -skeleton statistics with other cosmic web structure finders – e.g., friends-of-friends (FoF) (Davis et al. 1985), density-based techniques (Klypin & Holtzman 1997; Springel et al. 2001; Knollmann & Knebe 2009), T-web (Hahn et al. 2007; Forero-Romero et al. 2009), V-web (Hoffman et al. 2012; Forero-Romero et al. 2014), etc. Interesting points to address include the following: finding a value of β that yields a cosmic web realization similar to the one obtained with a different method; finding β for which the connections best trace the filament-like structures identified by a different realization of the cosmic web; using an alternative method to classify the cosmic web into clusters, filaments, walls, and voids, and study the statistical properties of the β -skeleton in those regions; using the β -skeleton statistics to study how the RSD effect varies in cluster, filament, wall, and void regions; etc.

Moreover, the β -skeleton can have several other applications in galaxy clustering analysis – being fast to compute and particularly sensitive to clustering properties. For example, it can be used to assess how well mocks can reproduce the properties of the observational sample, since it is sensitive to the strength and anisotropy of clustering. It can also be directly used to derive quantitative constraints on cosmological parameters, as the β -skeleton statistics are sensitive to the AP, volume, and RSD effects. This could be quantified by a β -correlation that compares the length of skeleton wedges built from data, randoms, and joint data/randoms:

⁴ The β -skeleton distribution can be thought as a ‘weighted’ 2PCF statistics, in which galaxy pairs are weighted by 0 or 1, respectively, based on a graphical criterion. One may be able to extract additional information from this particular weighting scheme.

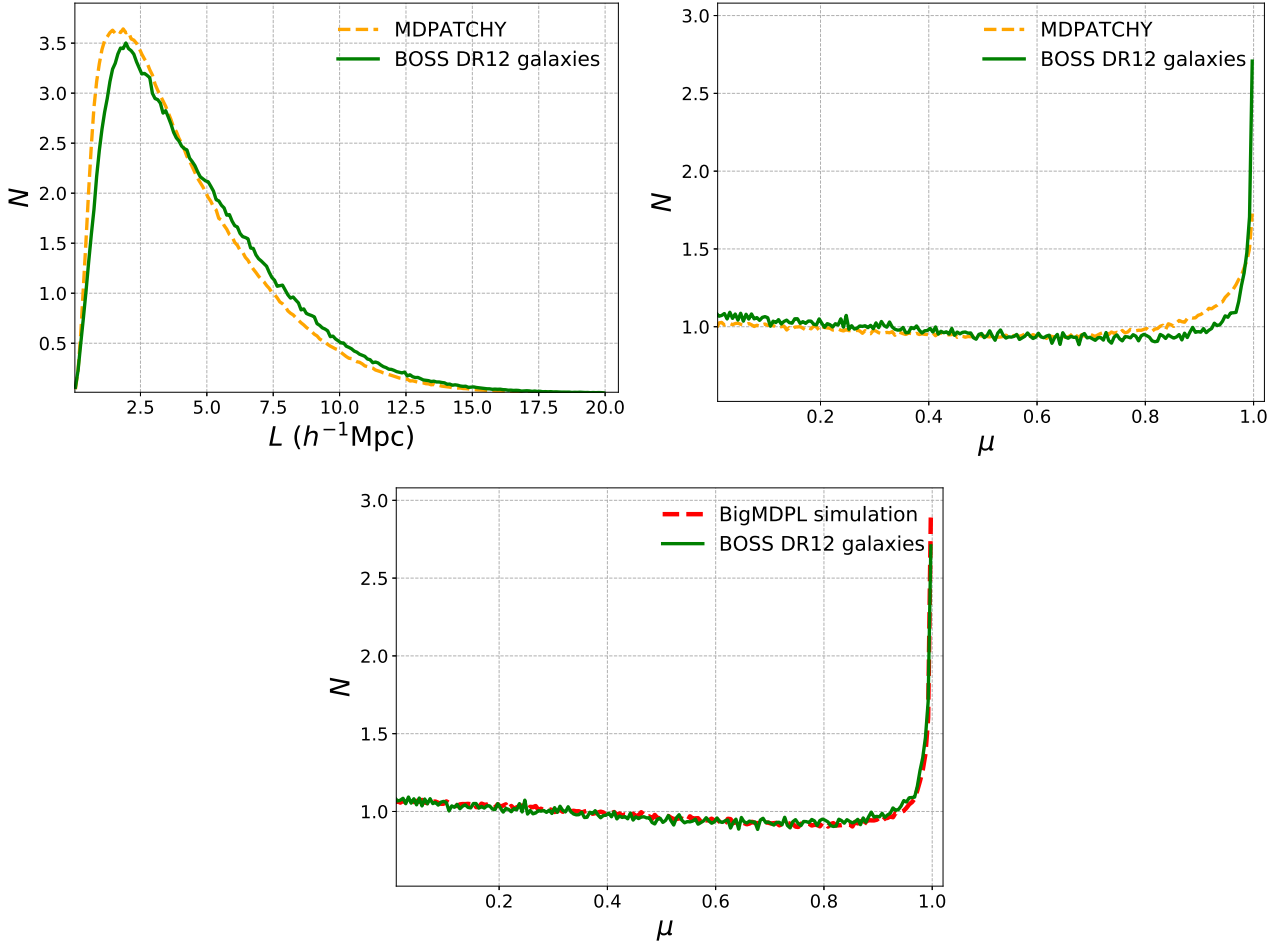


Figure 9. Comparisons between observed and simulated β -skeleton statistics. [Top left] Connection length distributions as measured from SDSS-III BOSS galaxy data (green solid line), and as derived from the Patchy mocks (dashed yellow line). [Top right] Same as in the left panel (also with identical line styles), but now for the distribution of the orientation directions; note that the Patchy mocks generally underestimate the FOG effect. [Bottom] Distribution of μ for SDSS-III BOSS galaxies (solid green line), and for the BigMDPL mock at $z = 0.6$ (red dashed line). The agreement between actual data and mocks is better in this case, as N -body simulations are capable of well-reproducing the RSD effect.

that function can be defined in such a way that in the limit $\beta \rightarrow 0$ converges to the two correlation function.

Finally, in this paper we only applied β -skeleton statistics to study the LSS, but this method can be refined and developed further along with other techniques in order to better characterize the properties of the cosmic web, and extract useful cosmological information.

ACKNOWLEDGEMENTS

J.E. F-R acknowledges support from COLCIENCIAS Contract No. 287-2016, Project 1204-712-50459. G.R. acknowledges support from the National Research Foundation of Korea (NRF) through Grant No. 2017R1E1A1A01077508 funded by the Korean Ministry of Education, Science and Technology (MoEST), and from the faculty research fund of Sejong University in 2018. F.L.L. acknowledges support from Key Program of National Natural Science Foundation of China (NFSC) through grant 11733010 and 11333008, and

the State Key Development Program for Basic Research of China (2015CB857000).

We greatly acknowledge Changbom Park for many helpful discussions.

References

- Alam S., et al., 2017, Monthly Notices of the Royal Astronomical Society, 470, 2617
- Amenta N., Bern M., Eppstein D., 1998, Graphical models and image processing, 60, 125
- Bardeen J. M., Bond J. R., Kaiser N., Szalay A. S., 1986, *ApJ*, 304, 15
- Barrow J. D., Bhavsar S. P., Sonoda D. H., 1985, *MNRAS*, 216, 17
- Bhardwaj M., Misra S., Xue G., 2005, in High Performance Switching and Routing, 2005. HPSR. 2005 Workshop on. pp 371–375
- Bos E. G. P., van de Weygaert R., Dolag K., Pettorino V., 2012, *MNRAS*, 426, 440

- Bose P., Devroye L., Evans W., Kirkpatrick D., 2002, in Latin American Symposium on Theoretical Informatics. pp 479–493
- Correa C. D., Lindstrom P., 2012, in Proceedings of the 18th ACM SIGKDD international conference on Knowledge discovery and data mining. pp 1330–1338
- Davis M., Efstathiou G., Frenk C. S., White S. D., 1985, *The Astrophysical Journal*, 292, 371
- Dawson K. S., et al., 2012, *The Astronomical Journal*, 145, 10
- Edelsbrunner H., Kirkpatrick D., Seidel R., 1983, *IEEE Transactions on information theory*, 29, 551
- Ersoy O., Hurter C., Paulovich F., Cantareiro G., Telea A., 2011, *IEEE Transactions on Visualization and Computer Graphics*, 17, 2364
- Forero-Romero J., Hoffman Y., Gottlöber S., Klypin A., Yepes G., 2009, *Monthly Notices of the Royal Astronomical Society*, 396, 1815
- Forero-Romero J. E., Contreras S., Padilla N., 2014, *Monthly Notices of the Royal Astronomical Society*, 443, 1090
- Guzzo L., et al., 2014, *A&A*, 566, A108
- Hahn O., Porciani C., Carollo C. M., Dekel A., 2007, *Monthly Notices of the Royal Astronomical Society*, 375, 489
- Hoffman Y., Metuki O., Yepes G., Gottlöber S., Forero-Romero J. E., Libeskind N. I., Knebe A., 2012, *Monthly Notices of the Royal Astronomical Society*, 425, 2049
- Huchra J. P., et al., 2012, *ApJS*, 199, 26
- Jackson J., 1972, *Monthly Notices of the Royal Astronomical Society*, 156, 1P
- Kaiser N., 1987, *Monthly Notices of the Royal Astronomical Society*, 227, 1
- Kirkpatrick D. G., Radke J. D., 1985, in , Vol. 2, *Machine Intelligence and Pattern Recognition*. Elsevier, pp 217–248
- Kitaura F.-S., et al., 2016, *Monthly Notices of the Royal Astronomical Society*, 456, 4156
- Klypin A., Holtzman J., 1997, arXiv preprint astro-ph/9712217
- Klypin A., Yepes G., Gottlöber S., Prada F., Hess S., 2016, *Monthly Notices of the Royal Astronomical Society*, 457, 4340
- Knollmann S. R., Knebe A., 2009, *The Astrophysical Journal Supplement Series*, 182, 608
- Lafarge F., Alliez P., 2013, in *Computer Graphics Forum*. pp 225–234
- Lee J., Park D., 2009, *ApJ*, 696, L10
- Li X.-D., Park C., Forero-Romero J. E., Kim J., 2014a, *ApJ*, 796, 137
- Li X.-D., Park C., Forero-Romero J. E., Kim J., 2014b, *The Astrophysical Journal*, 796, 137
- Li X.-D., Park C., Sabiu C. G., Kim J., 2015, *Monthly Notices of the Royal Astronomical Society*, 450, 807
- Libeskind N. I., et al., 2018, *MNRAS*, 473, 1195
- Reid B., et al., 2015, *Monthly Notices of the Royal Astronomical Society*, 455, 1553
- Rodríguez-Torres S. A., et al., 2016, *Monthly Notices of the Royal Astronomical Society*, 460, 1173
- Smee S. A., et al., 2013, *The Astronomical Journal*, 146, 32
- Sousbie T., 2011, *MNRAS*, 414, 350
- Springel V., White S. D., Tormen G., Kauffmann G., 2001, *Monthly Notices of the Royal Astronomical Society*, 328, 726
- Tegmark M., et al., 2004, *ApJ*, 606, 702
- Toussaint G., 2005, *International Journal of Computational Geometry & Applications*, 15, 101
- Wang Y., 2008, in , *Wireless sensor networks and applications*. Springer, pp 113–147
- Zhang W., King I., 2002, in *Neural Information Processing, 2002. ICONIP'02. Proceedings of the 9th International Conference on*. pp 1423–1427
- de Lapparent V., Geller M. J., Huchra J. P., 1986, *ApJ*, 302, L1
- van de Weygaert R., 2016, in van de Weygaert R., Shandarin S., Saar E., Einasto J., eds, *IAU Symposium Vol. 308, The Zeldovich Universe: Genesis and Growth*
- of the Cosmic Web. pp 493–523 ([arXiv:1611.01222](https://arxiv.org/abs/1611.01222)), [doi:10.1017/S1743921316010504](https://doi.org/10.1017/S1743921316010504)